

## Article

# Pseudo-Invariant Feature-Based Linear Regression Model (PIF-LRM): An Effective Normalization Method to Evaluate Urbanization Impacts on Land Surface Temperature Changes

Zhengwu Cai <sup>1</sup>, Chao Fan <sup>2</sup> , Falin Chen <sup>1</sup> and Xiaoma Li <sup>3,\*</sup>

<sup>1</sup> Hunan Provincial Key Laboratory of Rural Ecosystem Health in Dongting Lake Area, College of Resources and Environment, Hunan Agricultural University, Changsha 410128, China; caizhengwu@stu.hunau.edu.cn (Z.C.); chenfalinalin@hunau.edu.cn (F.C.)

<sup>2</sup> Department of Computer Sciences, University of Idaho, Moscow, ID 83844, USA; cfan@uidaho.edu

<sup>3</sup> Hunan Provincial Key Laboratory of Landscape Ecology and Planning & Design in Regular Higher Educational Institutions, College of Landscape Architecture and Art Design, Hunan Agricultural University, Changsha 410128, China

\* Correspondence: lixiaoma@hunau.edu.cn

**Abstract:** The Landsat land surface temperature (LST) product is widely used to understand the impact of urbanization on surface temperature changes. However, directly comparing multi-temporal Landsat LST is challenging, as the observed LST might be strongly affected by climatic factors. This study validated the utility of the pseudo-invariant feature-based linear regression model (PIF-LRM) in normalizing multi-temporal Landsat LST to highlight the urbanization impact on temperature changes, based on five Landsat LST images during 2000–2018 in Changsha, China. Results showed that LST of PIFs between the reference and the target images was highly correlated, indicating high applicability of the PIF-LRM to relatively normalize LST. The PIF-LRM effectively removed the temporal variation of LST caused by climate factors and highlighted the impacts of urbanization caused land use and land cover changes. The PIF-LRM normalized LST showed stronger correlations with the time series of normalized difference of vegetation index (NDVI) than the observed LST and the LST normalized by the commonly used mean method (subtracting LST by the average, respectively for each image). The PIF-LRM uncovered the spatially heterogeneous responses of LST to urban expansion. For example, LST decreased in the urban center (the already developed regions) and increased in the urbanizing regions. PIF-LRM is highly recommended to normalize multi-temporal Landsat LST to understand the impact of urbanization on surface temperature changes from a temporal point of view.

**Keywords:** spatiotemporal change; pseudo-invariant feature; relative normalization; urban expansion; urban heat island



**Citation:** Cai, Z.; Fan, C.; Chen, F.; Li, X. Pseudo-Invariant Feature-Based Linear Regression Model (PIF-LRM): An Effective Normalization Method to Evaluate Urbanization Impacts on Land Surface Temperature Changes. *Atmosphere* **2021**, *12*, 1540. <https://doi.org/10.3390/atmos12111540>

Academic Editor:  
Giridharan Renganathan

Received: 13 October 2021  
Accepted: 19 November 2021  
Published: 22 November 2021

**Publisher's Note:** MDPI stays neutral with regard to jurisdictional claims in published maps and institutional affiliations.



**Copyright:** © 2021 by the authors. Licensee MDPI, Basel, Switzerland. This article is an open access article distributed under the terms and conditions of the Creative Commons Attribution (CC BY) license (<https://creativecommons.org/licenses/by/4.0/>).

## 1. Introduction

Rapid urbanization changes land surface characteristics tremendously and causes significant increases in urban temperatures compared to the rural surroundings, which is also known as the urban heat island (UHI) effect. The UHI has significant ecological and environmental impacts such as disturbed terrestrial carbon dynamics [1,2], increased cooling energy consumption [3,4], and elevated risk of heat-related illness [5,6]. Nowadays the UHI is no longer a unique issue for large cities but is becoming a pressing environmental concern for medium- and even small-sized cities as well. It is not surprising that the number of UHI studies has increased exponentially over the last forty years [7].

Previous studies have identified urban expansion as one of the major drivers of surface temperature increases. Most of these studies have pointed out that (1) urban areas covered with buildings, roads, and other manmade features are warmer than the surrounding rural areas with natural land cover types; (2) hot areas are getting hotter, and areas with

high temperatures tend to expand spatially [8–11]. Most studies attribute these patterns to an extensive replacement of natural areas by impervious urban land cover. Yet how urban climate responds to the land cover changes that occurred at different stages of urban expansion has been largely overlooked. For example, the beginning phase of urbanization usually comes with a great decline of vegetated areas. Following the decline, there might be a recovery phase of vegetation as urban expansion unfolds [12,13]. As urban expansion and urban greening temporally interact with each other, the amount of vegetation may increase or decrease at different stages of urbanization. A thorough understanding of the coupled impacts of urban expansion and urban greening on the urban temperature is of great importance for better urban planning and management.

The Landsat land surface temperature (LST) product is among the most widely used datasets to study urban surface temperature changes. Because of its high spatial resolution, global spatial coverage, and more than 40 years of data archiving, the Landsat LST product has been frequently used to investigate the spatiotemporal variation of the urban climate in response to urban expansion [9,14–19]. However, unlike the Moderate-resolution Imaging Spectroradiometer (MODIS) LST data with daily observations, Landsat scans the Earth around twice per month, resulting in limited datasets, especially for regions with frequent rain and cloudy days. For some years, there is even no image that is usable to study the LST patterns. Moreover, it is challenging to investigate the urbanization impact on surface temperatures using the Landsat LST data, because the observed changes in the LST often contain multiple signals, including the effects of land use and land cover (LULC) change (e.g., urban expansion), climate variations (e.g., seasonal variation, daily variation), and some other effects. Taking a weather station in Changsha, China, as an example, Figure 1 shows a time series of the daily maximum air temperature (grey circles in Figure 1a) and daily MODIS LST (grey circles in Figure 1b) observed for the weather station for the period from 2000 to 2020. From the figure, both the air temperature and the MODIS LST display strong intra-annual variations, but very minimal inter-annual variations, as the fitted regression line for both graphs is almost flat (grey line in Figure 1a,b). To compare their data values with Landsat LST, we selected five days within the time series when Landsat LST images were available. We then obtained air temperature recordings and MODIS LST collected at the same day around the same time. The red dots in Figure 1b represent the five Landsat LST observations, and the blue dots in Figure 1a,b represent the air temperature and MODIS LST, respectively. Both air temperature and the two LSTs for the selected days show a completely different temporal trend than that with the daily temperature. The Landsat LST data points show a strong annual LST increase of more than 20 K. It is doubtful that the more than 20 K temperature increase is caused by the LULC change in the city alone. Therefore, there is a significant amount of uncertainty if we were to use the Landsat LST of the selected days directly to investigate the urbanization effects. In this example, the impacts of urbanization in Changsha would be significantly overestimated by using the raw Landsat LST in several selected days without any adjustment.

Relative normalization methods have been adopted to correct the “unexpected” signals in the LST images. The two most commonly used normalization methods are the centralization method (subtracting the pixel values by the average of the study area, called MEAN hereafter) [18,20,21] and the minimum–maximum normalization method [9,22]. Similar to the histogram matching method, the MEAN method subtracts the average of each LST image from its original values. The minimum–maximum normalization method normalizes each LST image to a range of 0 to 1. Despite these methods being the most commonly adopted, they have limitations, as they normalize LST solely based on the spatial variation of LST in each individual image and fail to consider the impacts from temporal LST changes over time.

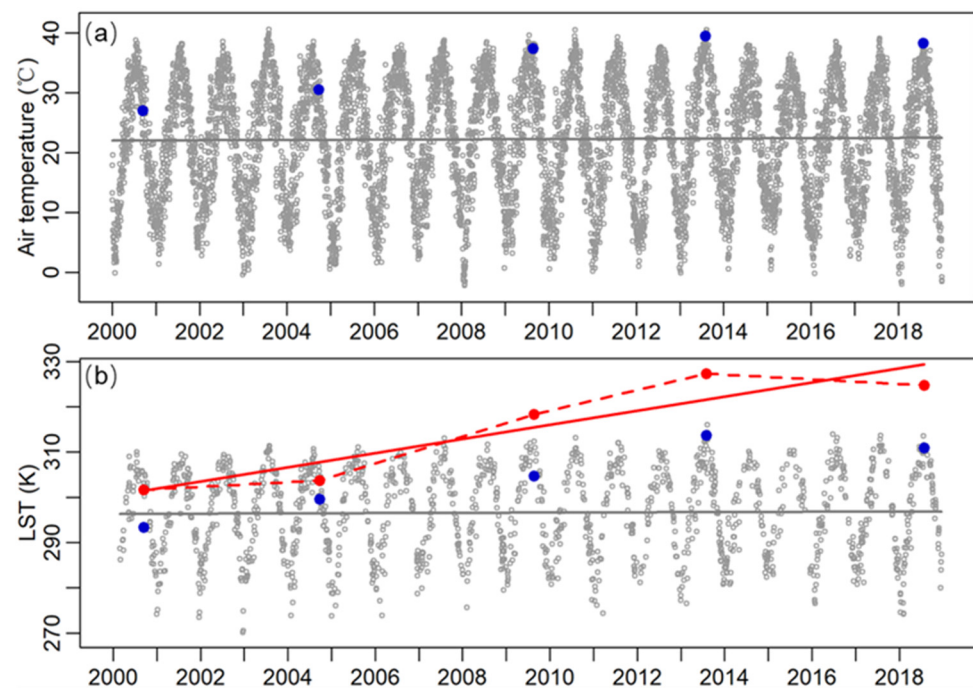


**Figure 1.** Time series of daily maximum air temperature (a) and MODIS Terra daytime LST (b) for a weather station in Changsha, China, from 2000 to 2020. The grey lines are the fitted linear regression lines; the blue points are air temperature and MODIS LST for the days when Landsat LSTs are available; the red points are Landsat LST of the selected days.

The pseudo-invariant feature (PIF)-based linear regression method, hereafter referred to as the PIF-LRM, is a temporally relative normalization method that addresses the limitations of the spatially relative normalization method as mentioned above. The PIF-LRM assumes the observed radiometric changes in different dates are caused by a range of factors including LULC change, atmospheric factors (i.e., annual variation, seasonal variation, daily variation, and diurnal variation), and other random effects. The atmospheric effects are homogeneous across the study area and can be modeled using a linear regression model [23–25]. The PIF-LRM has been successfully applied to temporally normalize vegetation index (e.g., normalized difference of vegetation index (NDVI)) [26], nighttime light images [27], and LST images [28]. For instance, Rajasekar and Weng [28] applied the PIF-LRM to normalize multi-temporal LST images for a better understanding of the spatiotemporal UHI pattern in Indianapolis, USA. Rahman, Hay, Couloigner, Hemachandran and Bailin [21] demonstrated that the PIF-LRM is effective in normalizing high-resolution thermal infrared airborne images of different flight lines for mosaicking. However, few studies have utilized the PIF-LRM normalized LST to study the impact of urbanization on urban surface temperatures.

Taking Changsha, a rapidly urbanizing city in China as a case study, we aimed to evaluate the performance of the PIF-LRM method in temporally normalizing LST. Taking five Landsat LST images from 2000 to 2018, we compared the effectiveness of the PIF-LRM and the widely used MEAN method in characterizing the LST changes in Changsha. The comparative study was conducted at three scales: study area, zones with different urbanization stages, and representative function zones. Findings of this study can help better understand the spatiotemporal evolution of urban temperature as a result of the LULC change, and provide guidelines for sustainable city development and management under rapid urban expansion.

## 2. Study Area and Dataset

### 2.1. Study Area

Changsha (112.59 E, 28.12 N), the capital city of Hunan province, is located in southeast China (Figure 2). It has a subtropical monsoon climate with an annual temperature of 17.2 °C and annual precipitation of 1361.6 mm. Changsha has long and hot summers with ~85 days warmer than 30 °C and ~30 days warmer than 35 °C in a year. There are three major rivers (i.e., Xiangjiang river, Liuyang river, and Laodao river) flowing through the city. Changsha is home to 7.92 million people and generated a gross domestic product of 1053.55 billion CNY in 2017. Changsha has experienced rapid urban expansion with the urbanization rate (percent urban population) increasing from 20.5% in 1978 to 77.6% in 2017 and the urban built-up area expanding from 53 km<sup>2</sup> in 1978 to 435 km<sup>2</sup> in 2017 [29]. Accompanying the rapid urbanization is the intensified surface UHI, which increased from 3.1 °C in 1994 to 4.5 °C in 2015 based on the remote sensing monitoring [30]. The policy of urban greening has been designed and implemented to mitigate the UHI. Our study area is the most developed region in the city (i.e., the area within the third ring road) with an area of ~680 km<sup>2</sup> (Figure 2). Water was excluded in our analysis.

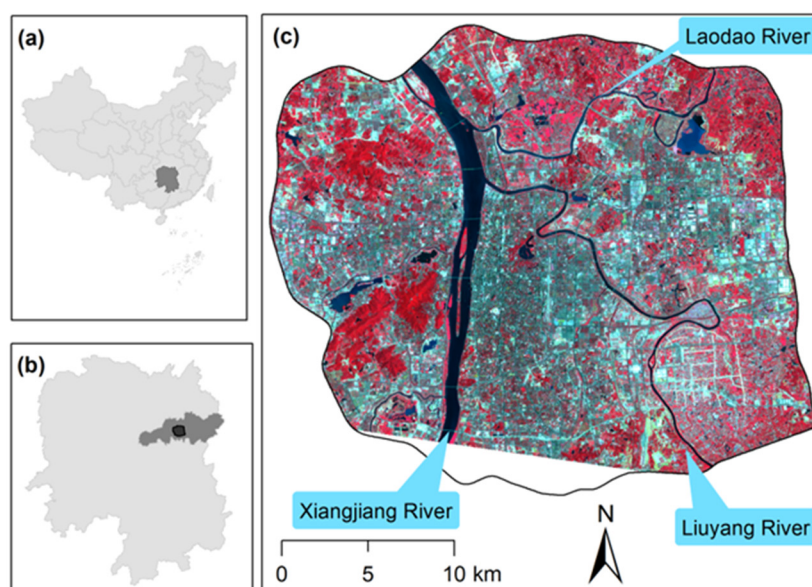


**Figure 2.** Study area: location of Hunan province in China (a), location of the study area in Changsha City and Hunan province (b), and Landsat image of the study area in 2018 (c).

### 2.2. Dataset

Landsat Collection 2 Level-2 Science Product from USGS (i.e., surface reflectance and surface temperature) was used for the LST. According to the Landsat Collection 2 Level 2 Science Product Guide, the LST was generated using the Landsat single channel surface temperature algorithm (Version 1.3.0). Three Landsat 5 Thematic Mapper (TM) images, namely from 2000 (13 September), 2004 (24 September), and 2009 (21 August); and two Landsat 8 Operational Land Imager (OLI) images, namely from 2013 (31 July) and 2018 (29 July), were acquired from the U.S. Geological Survey (USGS). These data were selected based on the principles of (1) cloud-free, (2) taken in hot months (in summer or early fall), and (3) close time interval (about 4–5 years). We used images of path 123 and row 40, which covers almost the entire study area except for a small fraction in the south (Figure 2). Figure 3 displays the selected Landsat images, and Supplementary Table S1 shows properties of these images.

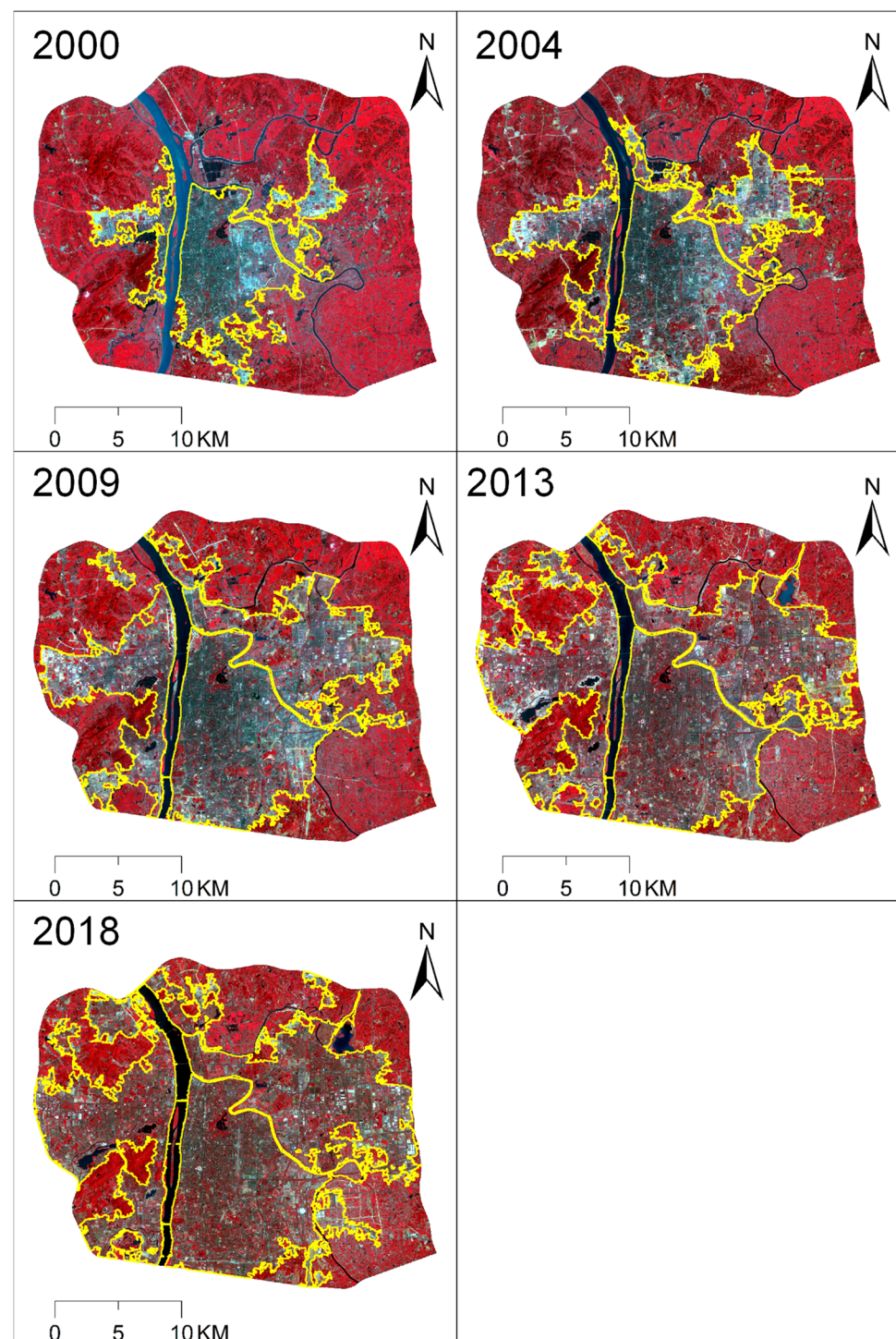


**Figure 3.** False color composite of Landsat images for selected years (the yellow lines indicate urban boundary).

### 3. Methods

Our methods include three steps (i.e., mapping urban expansion, normalizing LST, and validation). Figure 4 shows the flowchart of the methodology.

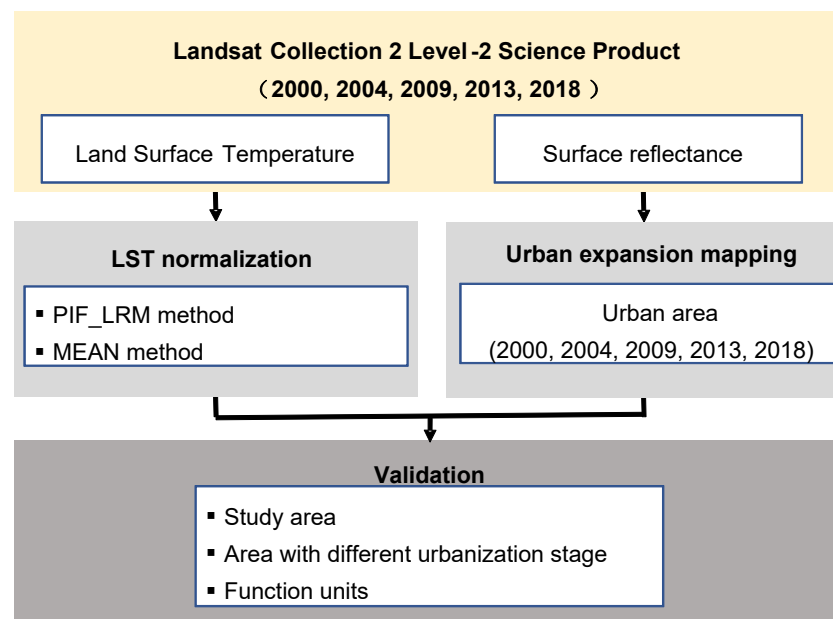


**Figure 4.** Workflow of the study.

### 3.1. Mapping Urban Expansion

To identify areas with different urbanization stages, we mapped urban expansion in the selected five years based on the Landsat images. First, we classified the Landsat image into three land cover classes (i.e., developed impervious land, vegetation, and water) based on the threshold method [31]. Water was firstly mapped by the modified normalized difference water index (MNDWI) [32], then vegetation was mapped by NDVI, and the remaining land cover was classified as developed impervious land because there is little bare land during the growing season. From the developed impervious land class, we removed the rural settlements such as the small patches far away from the city based on the high-resolution images from Google Earth. Finally, we reclassified the undeveloped lands that are surrounded by the identified developed land in the previous step as urban. For example, the urban parks and lakes in the highly developed area were treated as urban because they are important components of the urban ecosystem. The urban extent is analogous to previous studies focusing on the city-level UHI [33–36]. The accuracies of the mapped urban areas in the five years were 97%, 94%, 96%, 98%, and 93% for 2000, 2004, 2009, 2013, and 2018, respectively. The derived urban boundaries in each year are displayed in Figure 3, and Supplementary Figure S1 shows the urban area in different years.

### 3.2. Normalizing LST Using PIF-LRM

The PIF-LRM method takes the assumption that surface temperatures stay constant when no LULC change takes place. The differences, if they exist, should result from climate or systematic effects but not from LULC change [21,26,28]. We modeled the climate effect by performing the linear regression model between the PIFs of the target and the reference images. We identified the PIFs based on the NDVI and normalized difference building index (NDBI) of the reference and target images. We first calculated the absolute difference of the metrics between the target and reference images (2009 in this study). Then we selected pixels that fell within the 10th quantile of the absolute difference for both the NDVI and NDBI. Finally, we obtained the intersection of these two sets of pixels and treated them as PIFs. This ensured that the selected PIFs had few NDVI and NDBI changes between the reference and target images.

With the identified PIFs, we built linear regression models shown in Equation (1).

$$LST_{PIF(r)} = a + b \times LST_{PIF(t)} + \varepsilon_r \quad (1)$$

where  $LST_{PIF(r)}$  and  $LST_{PIF(t)}$  are the LST of the PIFs in the reference and target images, respectively,  $a$  and  $b$  are regression coefficients, and  $\varepsilon_r$  is the residual. We selected 2009 as the reference year because it was in the middle of the study period. All other years were corrected in reference to the 2009 image. Once the regression coefficients were estimated, the fitted regression model was then applied to the whole target image (Equation (2)).

$$LST_n = a + b \times LST_t \quad (2)$$

where  $LST_n$  is the temporally normalized LST, and  $LST_t$  is the observed or raw LST in the target year.

### 3.3. Validation

We tested the effectiveness of the PIF-LRM method by studying the temporal LST changes at three scales—study area, zones of different urbanization stages, and representative functional units. Then, we examined the temporal patterns of the PIF-LRM normalized LST in comparison with the observed LST and MEAN normalized LST. Finally, we evaluated the consistency and statistical relationship of the PIF-LRM normalized LST with the NDVI.

## 4. Results

### 4.1. Urban Expansion

Based on our mapping results, Changsha experienced rapid urban expansion with its urban areas increases of 218% from 124 km<sup>2</sup> in 2000 to 396 km<sup>2</sup> in 2018 (Figure 5a). There was a greater rate of urban expansion from 2000 to 2009, and the rate declined after 2009. The urban expansion followed a pancake-shaped spatial form, especially east of the Xiangjiang River (Figure 5b). Comparatively, the urban areas west of the Xiangjiang River were fragmented due to the Yuelu Mountains.

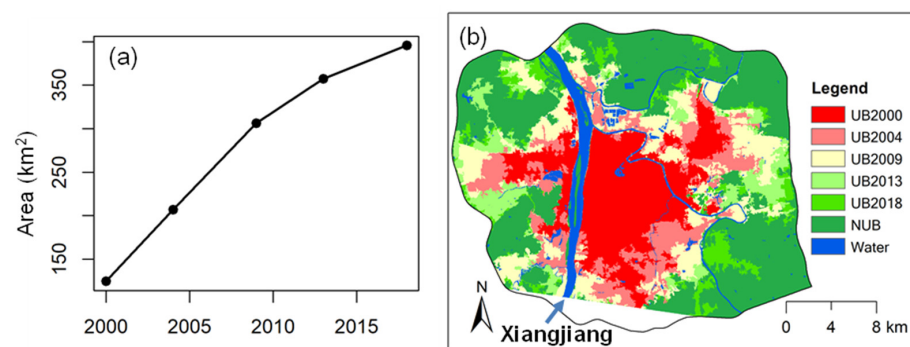


**Figure 5.** Urban area increase from 2000 to 2018 (a), and spatial distribution of urban expansion (b). (UB 2000: urban area before 2000; UB 2004: area urbanized between 2000 and 2004; UB 2009: area urbanized between 2004 and 2009; UB 2013: area urbanized between 2009 and 2013; UB 2018: area urbanized between 2013 and 2018; NUB: non-urban (natural) land in 2018).

### 4.2. Statistical Relationship of the LST between the Reference and Target PIFs

Following our PIF selection scheme, the total number of selected PIFs was 12,753 (2000), 13,699 (2004), 12,766 (2013), and 13,543 (2018). All PIFs were evenly distributed in the study area (Figure 6).

Figure 7 shows the scatterplots for LST between the reference and target PIFs. All relationships were significantly positive with an  $R^2$  higher than 0.75. There was a high degree of consistency in the LST of the selected PIFs between the reference and target images, indicating that the assumption of the PIF-LRM is fully satisfied and that the PIF-LRM can be applied to normalize Landsat LST.

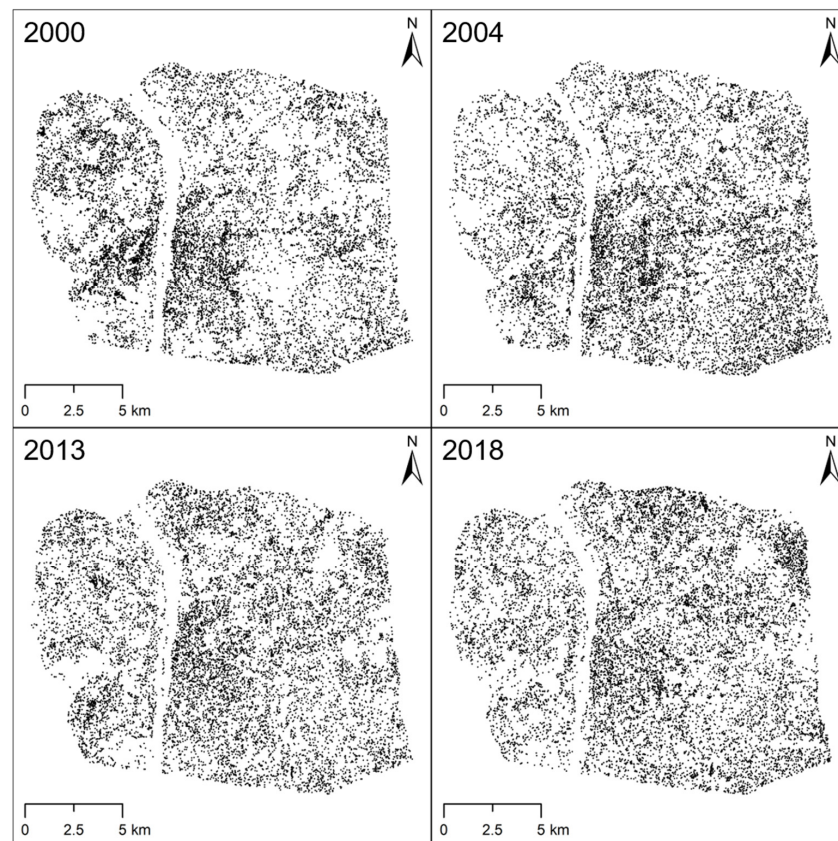


Figure 6. Spatial distribution of the PIFs for 2000, 2004, 2013, and 2018.

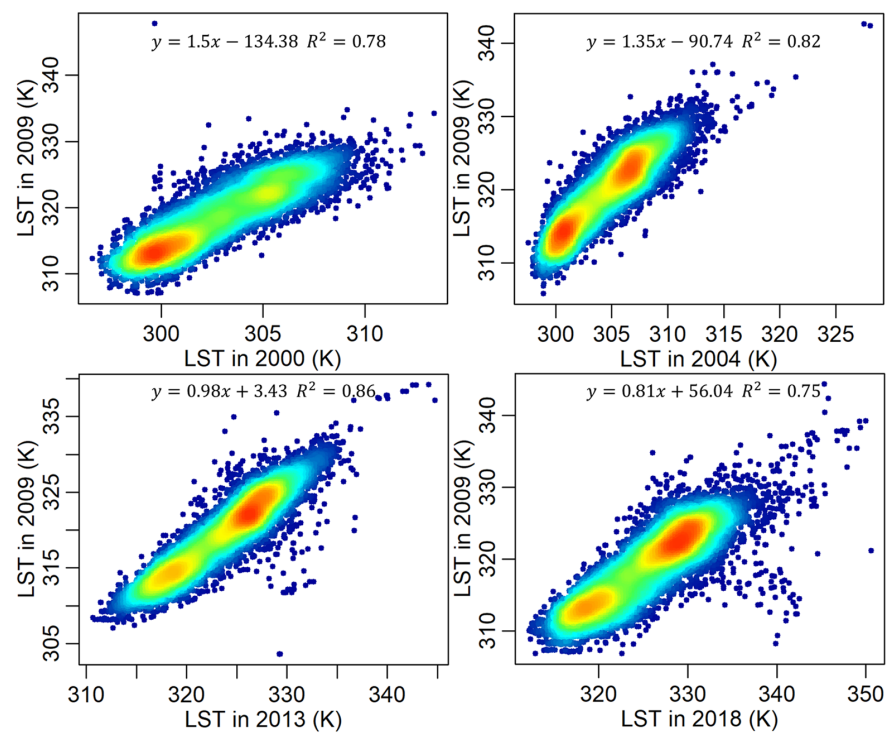
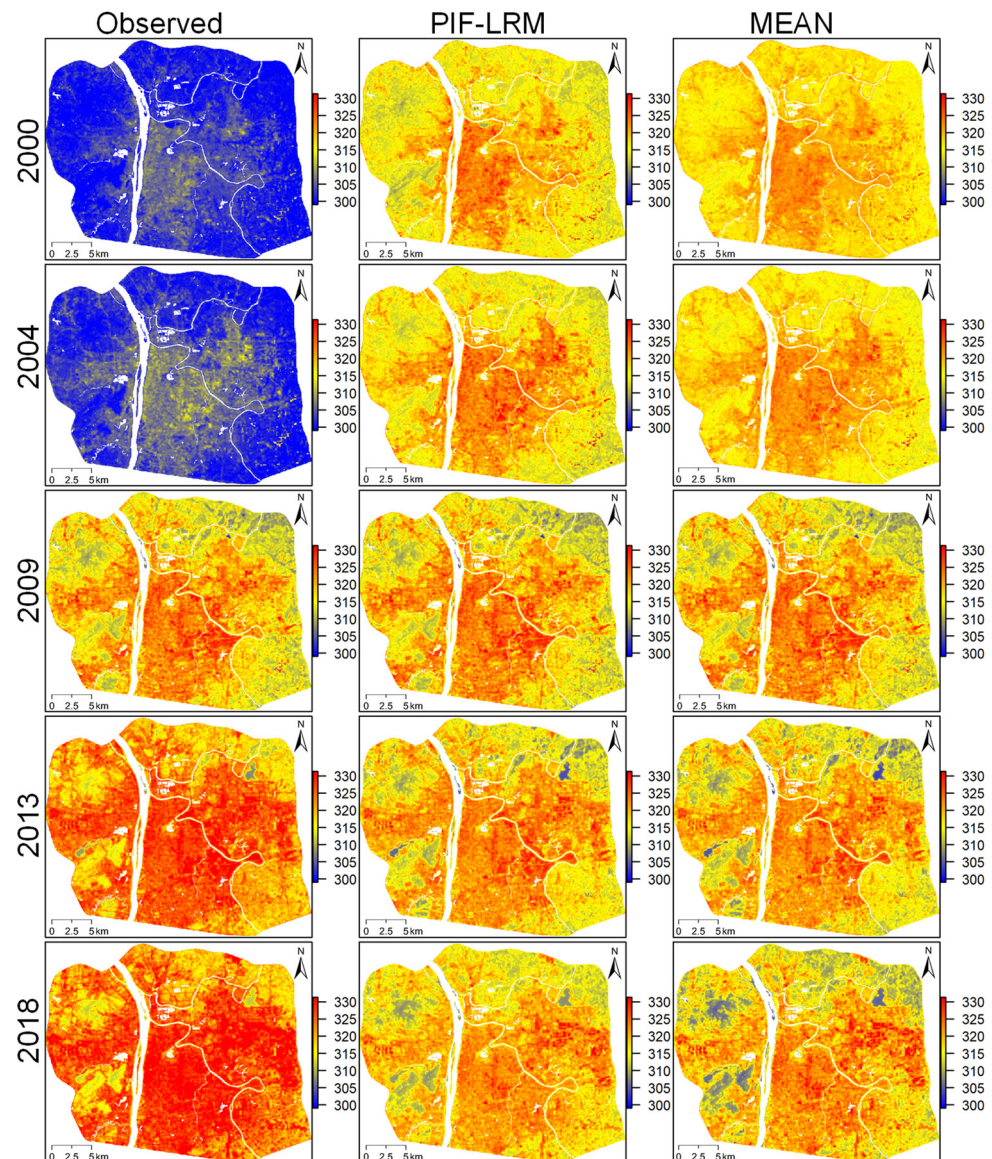


Figure 7. Scatterplot for LST of the PIFs between the target image (X-axis) and the reference image (Y-axis), the color indicates the density of points, red indicates the high density and blue indicates low density.

### 4.3. Validating the PIF-LRM at the Study Area Level

Figure 8 shows the PIF-LRM normalized LST images (middle) along with the observed LST (left) and the MEAN normalized LST (right). We can see that compared to the normalized LST images (middle and right), the observed LST (left) showed much greater LST changes during the time period. The observed LST was remarkably lower than the normalized LSTs in 2000 and 2004 and was significantly higher than the other two in 2013 and 2018. There was a more than 20 K temperature increase in the observed average LST for the study period. Multiple factors could have contributed to this large LST increase, but it is highly unlikely that the temperature increase was caused by urban expansion alone. The PIF-LRM and MEAN methods showed similar results with a consistently increasing LST over the years.



**Figure 8.** Observed Landsat LST (left column), PIF-LRM normalized LST (middle column), and MEAN normalized LST (right column).

To further compare the LSTs, we plotted the averaged observed LST, PIF-LRM normalized LST, and MEAN normalized LST for the years selected. We then plotted the averaged NDVI on the same graph (Figure 9). Again, we observed a great increase in the observed LST, going from 301.97 in 2000 to 325.22 in 2018. The regional averaged LST by the PIF-LRM

increased about 2 K, and the LST by the MEAN method stayed stable during the study period (Figure 9). A correlation analysis was conducted to further quantify the statistical relationship between the LSTs and the NDVI, which serves as a proxy of the LULC change in the study area. There was a strong negative relationship between the NDVI and the PIF-LRM normalized LST ( $r = -0.94$ ,  $p < 0.05$ ), followed by the observed LST ( $r = -0.68$ ,  $p > 0.05$ ) and the MEAN normalized LST ( $r = 0.57$ ,  $p > 0.05$ ). Compared with the other two LSTs, the very strong relationship between the PIF-LRM normalized LST and the NDVI indicates that the variations in the PIF-LRM normalized LST were closely associated with the LULC change in the region. It should therefore be used in place of the raw LST to study urbanization impacts on the urban surface temperature.

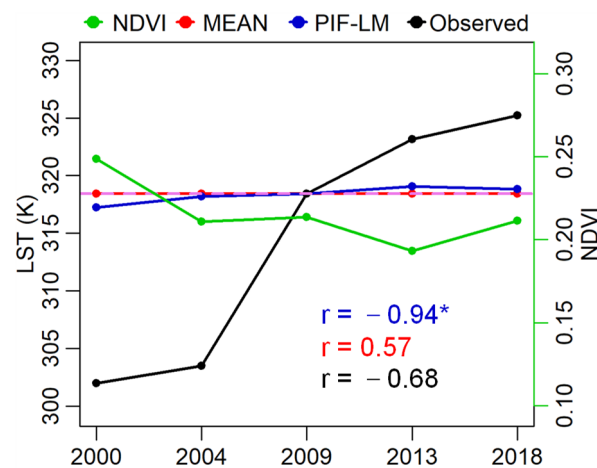


**Figure 9.** Temporal changes of observed LST (black line), PIF-LRM normalized LST (blue line), MEAN normalized LST (red line), and NDVI (green line) for the study area. The purple dashed line indicates the observed LST in 2009. \* indicates  $P < 0.05$ .

#### 4.4. Validating PIF-LRM at the Zonal Level with Different Urbanization Stages

To analyze the temporal changes by urbanization stage, we created the line charts for urban areas before 2000 (UB2000), areas urbanized between 2000 and 2004 (UB2004), areas urbanized between 2004 and 2009 (UB2009), areas urbanized between 2009 and 2013 (UB2013), areas urbanized between 2013 and 2018 (UB2018), and non-urban areas in 2018, respectively (Figure 10). Four metrics were plotted, including observed LST, PIF-LRM normalized LST, MEAN normalized LST, and NDVI. Based on the observed LST, all urbanization zones showed a consistently growing pattern with a total LST increase of more than 20 K. The greatest growth rate was observed during 2004 and 2009. Note that the observed LST increase was remarkable even for the already urbanized zone (UB2000) and non-urban areas (NUB), and the magnitude was comparable to other urbanization zones. With the normalization, the value of LST decreased significantly. Further, the rate of LST change for a particular urbanization zone (e.g., UB2009) was greatest for the urbanization period (e.g., 2004–2009). This indicates that there was indeed an LST increase in areas where urbanization takes place. The NDVI showed patterns consistent with the normalized LST, with the most notable declines occurring during the specific urbanization period. There was a strong negative relationship between the NDVI and PIF-LRM normalized LST for most urbanization zones, and the correlation was above 0.9 for UB2004, UB2013, and UB2018. The relationship was much weaker with the MEAN normalized LST, and all correlations were not significant except for UB2013. Note as well that for several zones, there was a certain degree of LST decline after the urbanization period (e.g., UB2009, UB2013). This might be attributed to an increase in urban greenspace after expansion, which was indicated by an NDVI increase for the same time period.

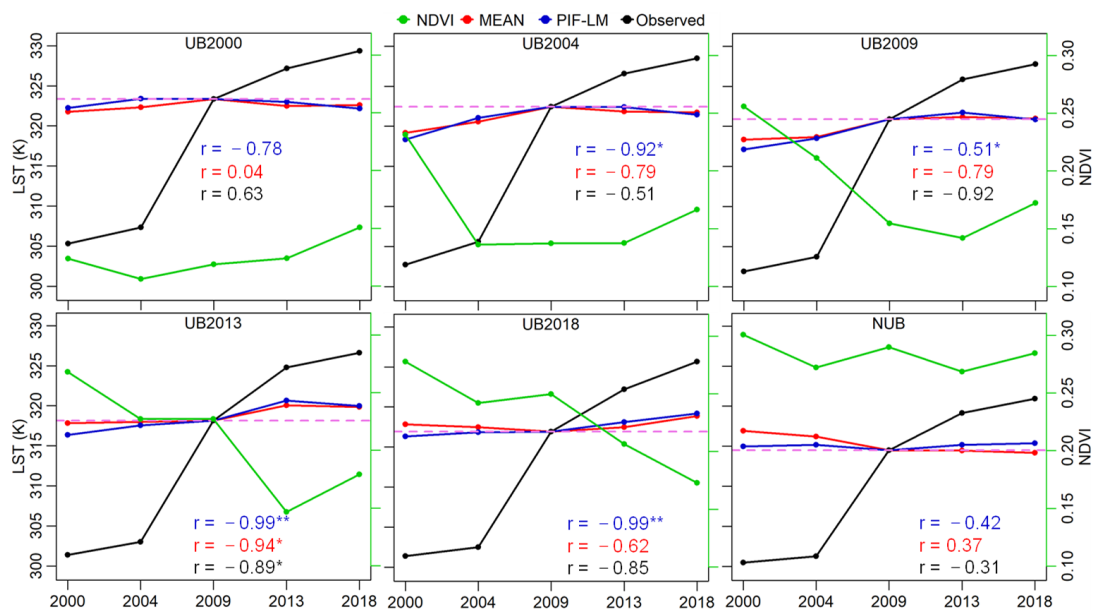


**Figure 10.** Temporal change of observed LST (black line), PIF-LRM normalized LST (blue line), MEAN normalized LST (red line), and NDVI (green line) for zones with different urbanization stages. The purple dashed line indicates the observed LST in 2009. Refer to the caption of Figure 2 for the full name of each zone. \* indicates  $P < 0.05$ , \*\* indicates  $P < 0.01$ .

#### 4.5. Validating PIF-LRM at the Local Level

For a better understanding of how the land conversion processes relate to the LST and NDVI changes, we picked three satellite scenes that respectively represented three land conversion scenarios (Figure 11). Figure 11a displays a place where natural lands were converted to industrial lands. Figure 11b shows the averaged observed LST, PIF-LRM normalized LST, MEAN normalized LST, and NDVI for the same place. There was a tremendous NDVI decrease during 2000–2004, when the most drastic land conversion occurred. The PIF-LRM normalized LST increased fast during this period and slowed down afterward (blue line in Figure 11b). The MEAN normalized LST, however, increased fast at first and continued to increase with nearly the same rate, even after the land cover change (red line in Figure 11b). It seems that the PIF-LRM normalization better captured the response of LST to LULC change than the MEAN normalized LST. Moreover, the relationship between NDVI and the PIF-LRM normalized LST was stronger than that between NDVI and the MEAN normalized LST and the observed LST.

The second example showed a place where farmland was converted to high-rise residential area with high vegetation coverage after 2008 (Figure 11c). The NDVI showed a “V”-shaped pattern with a decline between 2000 and 2009 and a continuous growth after 2009. Both the PIF-LRM and MEAN normalized LST showed a temporal pattern inverse of NDVI (i.e., increase first and then decrease). The PIF-LRM normalized LST had a stronger correlation with the NDVI than the MEAN normalized LST (Figure 11d). The third example shows a scenario where the industrial land was converted to a high-rise residential area (Figure 11e). The NDVI increased over the entire 18 years, and the normalized LSTs declined continuously (Figure 11f). The observed LST, however, showed a consistently growing pattern, which is unreasonable. We also observed a very strong positive relationship between the NDVI and observed LST, which might be due to climatic and other factors that were not effectively corrected before the analysis.

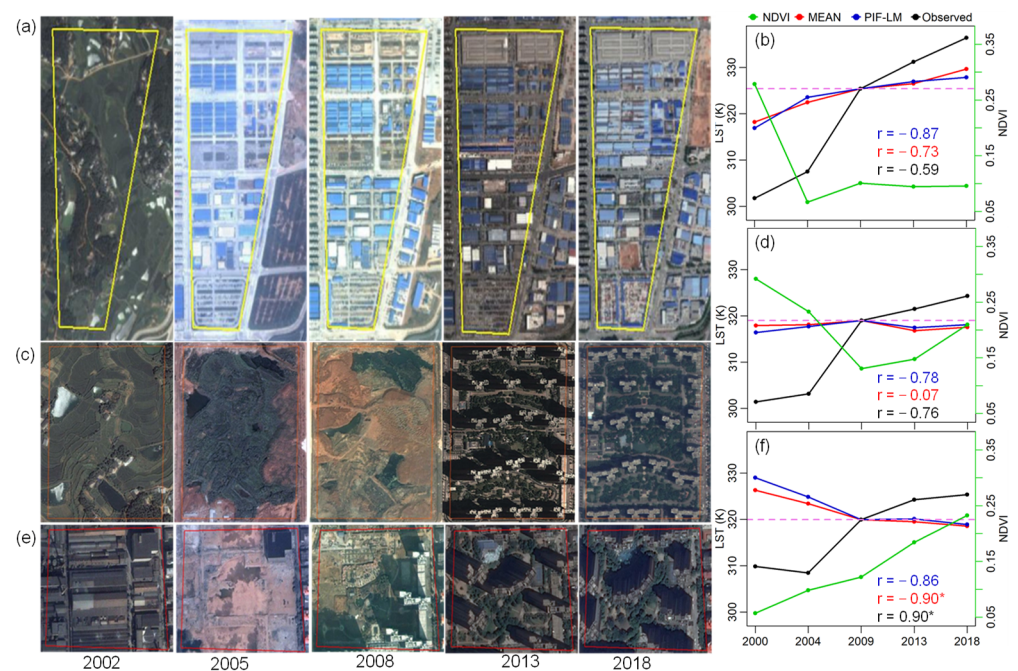


**Figure 11.** Land conversion (a,c,e) and the corresponding LST and NDVI change (b,d,f) for three example function units. Black line: observed LST; blue line: PIF-LRM normalized LST; red line: MEAN normalized LST; green line: NDVI. The purple dashed line indicates LST in 2009. \* indicates  $P < 0.05$ .

## 5. Discussion

Using directly observed LST to study the impact of urbanization on temperature change has been challenging. According to the observed LST, there was an average of more than a 20 K LST increase over a 700 km<sup>2</sup> region in Changsha from 2000 to 2018, which is highly unrealistic and questionable. Further, even the urban center developed before 2000 and the undeveloped land in 2018 witnessed a more than 20 K LST increase based on the observed LST. The direct use of the observed LST has been widely challenged in many previous studies, warranting the need for an effective technique to help address this issue [14,22,37].

We tested the performance of the PIF-LRM method in normalizing the LST at three levels. First, in contrast to the observed LST, the PIF-LRM effectively eliminated the systematic temporal shift of the LST that is not caused by urban expansion. There was a ~2 K LST increase for the study area during the study period compared to a more than 20 K LST increase according to the observed LST. Second, the temporal change of the normalized LST showed high consistency with the land cover change. For example, the urban center that developed before 2000 showed a decrease in the normalized LST after 2004 (Figure 10). This is possibly due to an increase in green vegetation, as indicated by an NDVI increase. Similar findings were reported in the trend analysis of the MODIS product, namely that when vegetation is recovering, the surface temperature in the urban center is decreasing [38–40]. Third, the time series of the normalized LST showed significant negative relationships with the NDVI, whereas the observed LST showed insignificant and even positive relationships with the NDVI.

Our results show that the PIF-LRM method is superior to the widely used MEAN method in normalizing Landsat LST. The MEAN method suggested that there was zero LST change in the study area over the 18 years, and the PIF-LRM method showed an LST increase of about 2 K (Figure 9). The latter estimation was corroborated by the LST increase (2.36 K) during 2001–2020 estimated by daily MODIS LST (unpublished data). In the analysis of the LST changes at the zonal level, there was a 2.76 K decrease in the MEAN normalized LST in the undeveloped zone (NUB) from 2000 to 2009 (Figure 10).

This decrease is likely not due to the LULC change but merely caused by a drawback of the MEAN method. Recall that the MEAN method subtracts the average of each LST image from its original LST value. Assuming that there is no temperature change for areas with no land conversions, the original LST values for the NUB region barely changed. However, the average observed LST in 2009 was higher than that in 2000 (Figure 9). This causes the MEAN normalized LST in 2009 to be smaller than that in 2000, which is a result of the normalization process and does not reflect the actual LST. Finally, the time series of the PIF-LRM normalized LST showed much stronger negative relationships with the NDVI than that of the MEAN normalized LST.

## 6. Conclusions

This study validated the effectiveness of the PIF-LRM in temporally normalizing Landsat LST to understand the impact of urbanization on urban temperature from a temporal point of view. Based on five Landsat LST images during 2000–2018, we showed that the temporal variations in the observed multi-temporal Landsat LST images contain information that is not solely caused by LULC change and therefore cannot be directly utilized to evaluate the urbanization-induced LST changes. Relative normalization methods are effective to remove the systematic shift of the LST among multi-temporal images. The PIF-LRM method provides a more accurate representation of the actual LST than the commonly used MEAN method. It better captures the spatially heterogeneous responses of the LST to urban expansion and should be widely adopted in future studies where multi-temporal LST images are utilized for a variety of purposes.

**Supplementary Materials:** The following are available online at <https://www.mdpi.com/article/10.3390/atmos12111540/s1>, Figure S1: Urban area in different years, Table S1: Properties of the used Landsat images (Collection 2 Level-2).

**Author Contributions:** C.F. and X.L. designed the research; Z.C., F.C. and X.L. analyzed the data; Z.C., C.F., F.C. and X.L. wrote the paper together. All authors have read and agreed to the published version of the manuscript.

**Funding:** This research was funded by National Natural Science Foundation of China (grant number 32001161), and the Hunan Provincial Natural Science Foundation of China (grant number 2021JJ30329).

**Institutional Review Board Statement:** Not applicable.

**Informed Consent Statement:** Not applicable.

**Data Availability Statement:** The data presented in this study are available upon request from the corresponding author.

**Acknowledgments:** We would like thank two anonymous reviewers for their constructive comments and suggestions, and the many colleagues and organizations that shared the data used in this project. The views and opinions expressed in this paper are those of the authors alone.

**Conflicts of Interest:** The authors declare no conflict of interest.

## References

1. Meineke, E.; Youngsteadt, E.; Dunn, R.R.; Frank, S.D. Urban warming reduces aboveground carbon storage. *Proc. R. Soc. B Biol. Sci.* **2016**, *283*, 20161574. [CrossRef]
2. Zhang, C.; Tian, H.; Pan, S.; Lockaby, G.; Chappelka, A. Multi-factor controls on terrestrial carbon dynamics in urbanised areas. *Biogeosci. Discuss.* **2014**, *11*, 17597–17631.
3. Li, X.; Zhou, Y.; Yu, S.; Jia, G.; Li, H.; Li, W. Urban heat island impacts on building energy consumption: A review of approaches and findings. *Energy* **2019**, *174*, 407–419. [CrossRef]
4. Azevedo, J.A.; Chapman, L.; Muller, C.L. Urban heat and residential electricity consumption: A preliminary study. *Appl. Geogr.* **2016**, *70*, 59–67. [CrossRef]
5. Cao, Q.; Yu, D.; Georgescu, M.; Wu, J.; Wang, W. Impacts of future urban expansion on summer climate and heat-related human health in eastern china. *Environ. Int.* **2018**, *112*, 134–146. [CrossRef] [PubMed]

6. Founda, D.; Santamouris, M. Synergies between urban heat island and heat waves in athens (greece), during an extremely hot summer (2012). *Sci. Rep.* **2017**, *7*, 10973. [CrossRef]
7. Zhou, D.; Xiao, J.; Bonafoni, S.; Berger, C.; Deilami, K.; Zhou, Y.; Frohling, S.; Yao, R.; Qiao, Z.; Sobrino, J.A. Satellite remote sensing of surface urban heat islands: Progress, challenges, and perspectives. *Remote Sens.* **2018**, *11*, 48. [CrossRef]
8. Waseem, S.; Khayyam, U. Loss of vegetative cover and increased land surface temperature: A case study of islamabad, pakistan. *J. Clean. Prod.* **2019**, *234*, 972–983. [CrossRef]
9. Grigoraş, G.; Urişescu, B. Land use/land cover changes dynamics and their effects on surface urban heat island in bucharest, romania. *Int. J. Appl. Earth Obs. Geoinf.* **2019**, *80*, 115–126. [CrossRef]
10. Peng, J.; Xie, P.; Liu, Y.; Ma, J. Urban thermal environment dynamics and associated landscape pattern factors: A case study in the beijing metropolitan region. *Remote Sens. Environ.* **2016**, *173*, 145–155. [CrossRef]
11. Wang, J.; Huang, B.; Fu, D.; Atkinson, P.M.; Zhang, X. Response of urban heat island to future urban expansion over the beijing–tianjin–hebei metropolitan area. *Appl. Geogr.* **2016**, *70*, 26–36. [CrossRef]
12. Zhou, W.; Wang, J.; Qian, Y.; Pickett, S.T.A.; Li, W.; Han, L. The rapid but “invisible” changes in urban greenspace: A comparative study of nine chinese cities. *Sci. Total Environ.* **2018**, *627*, 1572–1584. [CrossRef]
13. Sun, R.; Chen, L.; Braat, L.C. Effects of green space dynamics on urban heat islands: Mitigation and diversification. *Ecosyst. Serv.* **2017**, *23*, 38–46. [CrossRef]
14. Yu, Z.; Yao, Y.; Yang, G.; Wang, X.; Vejre, H. Spatiotemporal patterns and characteristics of remotely sensed region heat islands during the rapid urbanization (1995–2015) of southern china. *Sci. Total Environ.* **2019**, *674*, 242–254. [CrossRef]
15. Peres, L.D.F.; Lucena, A.J.D.; Rotunno Filho, O.C.; França, J.R.D.A. The urban heat island in Rio de Janeiro, Brazil, in the last 30 years using remote sensing data. *Int. J. Appl. Earth Obs. Geoinf.* **2018**, *64*, 104–116. [CrossRef]
16. Estoque, R.C.; Murayama, Y.; Myint, S.W. Effects of landscape composition and pattern on land surface temperature: An urban heat island study in the megacities of southeast asia. *Sci. Total Environ.* **2017**, *577*, 349–359. [CrossRef]
17. Estoque, R.C.; Murayama, Y. Monitoring surface urban heat island formation in a tropical mountain city using landsat data (1987–2015). *ISPRS J. Photogramm. Remote Sens.* **2017**, *133*, 18–29. [CrossRef]
18. Masoudi, M.; Tan, P.Y.; Fadaei, M. The effects of land use on spatial pattern of urban green spaces and their cooling ability. *Urban Clim.* **2021**, *35*, 100743. [CrossRef]
19. Zhang, H.; Li, T.-T.; Han, J.-J. Quantifying the relationship between land use features and intra-surface urban heat island effect: Study on downtown shanghai. *Appl. Geogr.* **2020**, *125*, 102305. [CrossRef]
20. Dutta, I.; Das, A. Exploring the spatio-temporal pattern of regional heat island (rhi) in an urban agglomeration of secondary cities in eastern india. *Urban Clim.* **2020**, *34*, 100679. [CrossRef]
21. Rahman, M.M.; Hay, G.J.; Couloigner, I.; Hemachandran, B.; Bailin, J. A comparison of four relative radiometric normalization (rrn) techniques for mosaicing h-res multi-temporal thermal infrared (tir) flight-lines of a complex urban scene. *ISPRS J. Photogramm. Remote Sens.* **2015**, *106*, 82–94. [CrossRef]
22. Yue, W.; Qiu, S.; Xu, H.; Xu, L.; Zhang, L. Polycentric urban development and urban thermal environment: A case of hangzhou, china. *Landsc. Urban Plan.* **2019**, *189*, 58–70. [CrossRef]
23. Schott, J.R.; Salvaggio, C.; Volchok, W.J. Radiometric scene normalization using pseudoinvariant features. *Remote Sens. Environ.* **1988**, *26*, 1–16. [CrossRef]
24. Du, Y.; Teillet, P.M.; Cihlar, J. Radiometric normalization of multitemporal high-resolution satellite images with quality control for land cover change detection. *Remote Sens. Environ.* **2000**, *82*, 123–134. [CrossRef]
25. Syariz, M.A.; Lin, B.-Y.; Denaro, L.G.; Jaelani, L.M.; Van Nguyen, M.; Lin, C.-H. Spectral-consistent relative radiometric normalization for multitemporal landsat 8 imagery. *ISPRS J. Photogramm. Remote Sens.* **2019**, *147*, 56–64. [CrossRef]
26. Chen, X.; Vierling, L.; Deering, D. A simple and effective radiometric correction method to improve landscape change detection across sensors and across time. *Remote Sens. Environ.* **2005**, *98*, 63–79. [CrossRef]
27. Wei, Y.; Liu, H.; Song, W.; Yu, B.; Xiu, C. Normalization of time series dmsp-ols nighttime light images for urban growth analysis with pseudo invariant features. *Landsc. Urban Plan.* **2014**, *128*, 1–13. [CrossRef]
28. Rajasekar, U.; Weng, Q. Spatio-temporal modelling and analysis of urban heat islands by using landsat tm and etm+ imagery. *Int. J. Remote Sens.* **2009**, *30*, 3531–3548. [CrossRef]
29. Hunan Daily. Urbanization Level Increased from 20.5% to 77.6% in Changsha for the Past 40 Years (1978–2017). 2018. Available online: <https://m.voc.com.cn/wxhn/article/201810/201810210851314915.html> (accessed on 21 November 2021).
30. Morning Hunan. Urban Heat Island in Changsha-Zhuzhou-Xiangtan in the Past 20 Years: Increased from 3 °C to 7.3 °C. 2016. Available online: <http://www.xxcb.cn/event/hunan/2016-06-23/9059122.html> (accessed on 21 November 2021).
31. Li, C.; Li, J.; Wu, J. Quantifying the speed, growth modes, and landscape pattern changes of urbanization: A hierarchical patch dynamics approach. *Landsc. Ecol.* **2013**, *28*, 1875–1888. [CrossRef]
32. Xu, H. Modification of normalised difference water index (ndwi) to enhance open water features in remotely sensed imagery. *Int. J. Remote Sens.* **2006**, *27*, 3025–3033. [CrossRef]
33. Li, X.; Zhou, W. Optimizing urban greenspace spatial pattern to mitigate urban heat island effects: Extending understanding from local to the city scale. *Urban For. Urban Green.* **2019**, *41*, 255–263. [CrossRef]
34. Zhou, D.; Zhao, S.; Liu, S.; Zhang, L.; Zhu, C. Surface urban heat island in china’s 32 major cities: Spatial patterns and drivers. *Remote Sens. Environ.* **2014**, *152*, 51–61. [CrossRef]

35. Zhou, D.; Bonafoni, S.; Zhang, L.; Wang, R. Remote sensing of the urban heat island effect in a highly populated urban agglomeration area in east china. *Sci. Total Environ.* **2018**, *628–629*, 415–429. [[CrossRef](#)]
36. Peng, J.; Ma, J.; Liu, Q.; Liu, Y.; Hu, Y.N.; Li, Y.; Yue, Y. Spatial-temporal change of land surface temperature across 285 cities in china: An urban-rural contrast perspective. *Sci. Total Environ.* **2018**, *635*, 487–497. [[CrossRef](#)]
37. Halder, B.; Bandyopadhyay, J.; Banik, P. Monitoring the effect of urban development on urban heat island based on remote sensing and geo-spatial approach in kolkata and adjacent areas, india. *Sustain. Cities Soc.* **2021**, *74*, 103186. [[CrossRef](#)]
38. Zhou, D.; Zhang, L.; Hao, L.; Sun, G.; Liu, Y.; Zhu, C. Spatiotemporal trends of urban heat island effect along the urban development intensity gradient in china. *Sci. Total Environ.* **2016**, *544*, 617–626. [[CrossRef](#)] [[PubMed](#)]
39. Yao, R.; Wang, L.; Huang, X.; Zhang, W.; Li, J.; Niu, Z. Interannual variations in surface urban heat island intensity and associated drivers in china. *J. Environ. Manag.* **2018**, *222*, 86–94. [[CrossRef](#)]
40. Xue, Y.; Lu, H.; Guan, Y.; Tian, P.; Yao, T. Impact of thermal condition on vegetation feedback under greening trend of china. *Sci. Total Environ.* **2021**, *785*, 147380. [[CrossRef](#)] [[PubMed](#)]